

Article

Mechanism of NO Photocatalytic Oxidation on g-C₃N₄ Was Changed by Pd-QDs Modification

Yuhan Li ¹, Liping Yang ², Guohui Dong ^{2,*} and Wingkei Ho ^{1,*}

Received: 1 December 2015; Accepted: 17 December 2015; Published: 26 December 2015

Academic Editor: Derek J. McPhee

¹ Department of Science and Environmental Studies, The Hong Kong Institute of Education, Tai Po, New Territories, Hong Kong, China; s1116421@s.ied.edu.hk

² Laboratory of Environmental Sciences and Technology, Xinjiang Technical Institute of Physics & Chemistry, and Key Laboratory of Functional Materials and Devices for Special Environments, Chinese Academy of Sciences, Urumqi 830011, China; yanglp@ms.xjb.ac.cn

* Correspondence: donggh@ms.xjb.ac.cn (G.D.); keithho@ied.edu.hk (W.H.); Tel.: +86-151-9915-3105 (G.D.); +852-2948-8255 (W.H.)

Abstract: Quantum dot (QD) sensitization can increase the light absorption and electronic transmission of photocatalysts. However, limited studies have been conducted on the photocatalytic activity of photocatalysts after modification by noble metal QDs. In this study, we developed a simple method for fabricating Pd-QD-modified g-C₃N₄. Results showed that the modification of Pd-QDs can improve the NO photocatalytic oxidation activity of g-C₃N₄. Moreover, Pd-QD modification changed the NO oxidation mechanism from the synergistic action of h⁺ and O₂[−] to the single action of ·OH. We found that the main reason for the mechanism change was that Pd-QD modification changed the molecular oxygen activation pathway from single-electron reduction to two-electron reduction. This study can not only develop a novel strategy for modifying Pd-QDs on the surface of photocatalysts, but also provides insight into the relationship between Pd-QD modification and the NO photocatalytic oxidation activity of semiconductor photocatalysts.

Keywords: quantum dot; g-C₃N₄; photocatalytic oxidation; NO

1. Introduction

Since Fujishima and Honda discovered oxygen and hydrogen evolution at a semiconductor electrode under light irradiation in 1972 [1], semiconductor photocatalysis have attracted worldwide attention in the fields of water or air purification [2–5], water splitting [6] and CO₂ photoreduction [7,8]. Over the past four decades, various photocatalysts, such as oxides, sulfides and oxynitrides, have been developed to utilize solar energy for environmental purification and energy conversion [9–12]. However, most of these materials can only be excited by ultraviolet (UV) light, which occupies only 4% of solar light. Therefore, many researchers turn to develop new photocatalysts that are active under visible light. Among these endeavors, Wang *et al.* [13] reported that graphitic carbon nitride (g-C₃N₄) can produce oxygen or hydrogen by water splitting under visible light irradiation. More importantly, this metal-free polymer can withstand acid alkalis and high temperature because of the strong covalent bonds between carbon and nitride atoms. These advantages make g-C₃N₄ one of the most significant catalysts in the field of photocatalysis [14–17]. To increase the efficiency of this attractive material, many methods, such as surface area enhancement, anionic or cationic doping and coupling with other semiconductors, have been developed by researchers [18–20]. Despite all of these properties, the visible light photocatalytic activity of g-C₃N₄ is still low because of the fast recombination of the photogenerated carriers. Therefore, more efficient methods for improving the visible light photocatalytic activity of g-C₃N₄ should be designed and developed.

Quantum dots (QD) are nanoparticles with a unique feature, *i.e.*, they can generate more than one electron for every absorbed photon. A recent report showed that QD sensitization could increase the light absorption and electronic transmission of photocatalysts. For example, C dots can enhance the performance of many photocatalysts, such as g-C₃N₄, TiO₂ and Bi₂MoO₆, because of their ultrafast electron transferability [21–23]. The presence of CdS-QDs can favor the electron transfer and enhance the photoactivity of Zn_{1-x}Cd_xS [24]. However, in all previous studies, the enhancement mechanism of photoactivity that is induced by the QDs sensitization is still in dispute. Some previous studies showed that the interfacial electron transfer from QDs to photocatalysts was due to the quantum confinement effect, whereas other previous studies consider that QDs can capture the photogenerated electrons and inhibit the recombination of electron-hole pairs [25,26]. Therefore, finding out how QDs will influence the photoreactivity of photocatalysts is considerably important, but challenging.

Some studies have demonstrated that the existence of noble metal on the surfaces of g-C₃N₄ particles could improve the photocatalytic activity of g-C₃N₄ by inhibiting the recombination of photoinduced electron-hole pairs [27–29]. However, few research works carefully studied the photocatalytic activity of g-C₃N₄ when it was modified by noble metal QDs. Although noble metals were often deposited on g-C₃N₄ surfaces, the sizes of these metals were larger than that of QDs. In view of the advantages of noble metals and QDs for g-C₃N₄ photocatalytic activity, we speculate that noble metal QD modification will be more effective than noble metal partials to improve the g-C₃N₄ photocatalytic activity. In this study, we have successfully prepared g-C₃N₄, which was modified with palladium QDs (PQDs), by a chemical reduction method for the first time. The resulting materials were carefully characterized and then used for the photocatalytic removal of organic NO under visible light irradiation. A series of experiments was designed to clarify the roles of PQDs on g-C₃N₄ photocatalysis under visible light. The reasons for the enhancement of the photocatalytic activity were analyzed in detail.

2. Experimental Section

2.1. Synthesis of Photocatalysts

Graphitic carbon nitride (g-C₃N₄) was prepared by calcining melamine in an alumina crucible with cover at 500 °C for 2 h and with an initial heating rate of 20 °C/min. This melamine was further calcined at 520 °C for 2 h. This procedure was similar to our previous paper [30].

PQDs-modified g-C₃N₄ was synthesized by an *in situ* chemical reduction method. In a typical synthetic procedure, the as-prepared g-C₃N₄ powder was added to 50 mL PdCl₂ solution (0.5 g/dm³). After 20 min, the suspension was centrifuged and washed by distilled water many times. Then, the suspension was added to 50 mL of NaH₂PO₂·2H₂O solution (20 g/dm³) under stirring. When it was stirred for 20 min, the suspension was centrifuged and washed thoroughly with distilled water. Finally, the sample was dried at 50 °C in a vacuum drying chamber. The final sample was denoted as PQDs-g-C₃N₄.

2.2. Characterization

The powder X-ray diffraction (XRD) patterns were recorded on a Bruker D8 Advance diffractometer (BRUKER, Berlin, Germany) with the DAVINCI design and monochromatized Cu K α radiation ($\lambda = 1.5418 \text{ \AA}$). Transmission electron microscopy (TEM) images were obtained on a JEOL JSM-2010 microscope (JEOL, Tokyo, Japan) with an accelerating voltage of 200 kV. The TEM samples were prepared by dispersing the final powders in ethanol, and then, the dispersion was dropped on lacey support film grids. UV-VIS diffuse reflectance spectra were obtained by using a UV-VIS spectrometer (Shimadzu UV-2550, Tokyo, Japan) with BaSO₄ as a reference, and these spectra were converted from reflection to absorbance by the Kubelka–Munk method. XPS measurements were performed in a VG scientific ESCALAB Mark II spectrometer (ESCALAB, London, UK), which was

equipped with two ultra-high vacuum chambers. All of the binding energies were calibrated to the C1s peak at 284.6eV of the surface adventitious carbon.

2.3. Photocatalytic Activity Test

The photocatalytic activities of the resulting samples were tested for the photocatalytic removal of NO under visible light irradiation. In the experiments, NO removal at ppb levels was performed at ambient temperature in a continuous flow reactor. The rectangular reactor with a volume of 4.5 L (30 cm × 15 cm × 10 cm (L × W × H)) was made of stainless steel and covered with quartz glass. One sample dish, which contained the g-C₃N₄ or PQDs-g-C₃N₄ film, was placed in the middle of the reactor. A LED lamp (λ = 448 nm), which was vertically placed outside of the reactor above the sample dish, was used as the visible light source.

g-C₃N₄ and PQDs-g-C₃N₄ films were prepared by coating an aqueous suspension of g-C₃N₄ or PQDs-g-C₃N₄ onto a glass dish with a diameter of 12 cm. g-C₃N₄ or PQDs-g-C₃N₄ (0.15 g) was added to 15 mL of H₂O and ultrasonicated for 20 min. Subsequently, the aqueous suspension was coated onto the glass dish, which was then dried at 60 °C until the water was completely removed.

NO gas was obtained from a compressed gas cylinder with traceable National Institute of Standards and Technology specifications. The NO concentration was diluted to about 600 ppb by the air stream that was supplied by a zero air generator. The flow rate was controlled at 1 L/min by a mass flow controller. After the adsorption–desorption equilibrium among gases and photocatalysts was achieved, the lamp was turned on. The NO concentration was continuously measured by using a Model T200 chemiluminescence NO analyzer (Teledyne, Thousand Oaks, CA, USA). NO removal efficiency (η) was calculated as follows:

$$\eta (\%) = (1 - C/C_0) \times 100\%$$

where C and C₀ are the concentrations of NO in the outlet stream and the feeding stream, respectively.

2.4. Trapping Experiment

Active species trapping experiments were performed to investigate the NO removal mechanism. Potassium iodide (KI) and *tert*-butyl alcohol (TBA) were chosen as hole and ·OH scavengers, respectively. Argon was used to remove oxygen during the photocatalytic process. Typically, 0.15 g of photocatalyst with different trapping agents was added into 15 mL of H₂O and ultrasonicated for 20 min. The aqueous suspensions were then coated onto the sample dish. Subsequently, the coated dish was dried at 60 °C until the water was completely removed. Finally, the coated dishes were used in NO removal experiments.

To eliminate the effect of H₂O₂, 1 mg · L⁻¹ H₂O₂ was added into the sample dish under visible light in the absence of photocatalyst. Then, the NO concentration was measured by the NO analyzer.

3. Results and Discussion

3.1. Structural Characterization of Result Samples

XRD was used to characterize the phase structure of the products. Figure 1 shows the powder XRD patterns of the as-prepared samples, where two peaks are found in all of the samples. The small angle peak at 13.08°, which corresponded to 0.676 nm, was due to the stacking of the interlayer. The strongest peak at 27.41°, which corresponded to 0.326 nm, was due to the stacking of the conjugated aromatic system that was indexed as the (002) peak for graphitic materials. No other peaks, such as Pd, could be detected in the XRD pattern of PQDs-g-C₃N₄, which indicates that the content of deposited Pd was considerably low to determine its existence and that Pd was dispersed uniformly onto the g-C₃N₄ surfaces.

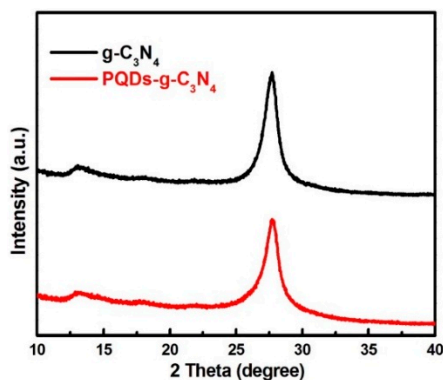


Figure 1. The powder XRD patterns of the as-prepared samples. PQD, palladium QD.

X-ray photoelectron spectroscopy (XPS) was used to investigate the chemical compositions of the photocatalyst structures. Figure 2a shows the survey spectra of the two resulting samples, in which $g\text{-C}_3\text{N}_4$ was composed of two elements, C and N, whereas $\text{PQDs-g-C}_3\text{N}_4$ was composed of three elements, C, N and Pd. As shown in Figure 2b, the C 1s spectrum could be fitted with two peaks at binding energies of 284.6 and 288.2 eV for both $g\text{-C}_3\text{N}_4$ and $\text{PQDs-g-C}_3\text{N}_4$, which is indicative of two different carbons in these two samples. The major peak at 288.2 eV was ascribed to the existence of sp^2 -hybridized carbon in C–N–C coordination, whereas the peak at 284.6 eV was assigned to the surface adventitious carbon. In the N 1s spectrum, the spectra of both samples could be separated into three binding energies (Figure 2c). The strongest peak at 398.7 eV could be assigned to sp^2 -hybridized nitrogen in the C–N–C groups. The peak at 400.2 eV was usually attributed to the tertiary nitrogen N–C₃ groups. The weak additional signal at 401.3 eV could be attributed to the amino functional groups with hydrogen (C–N–H), which might be related to structural defects and incomplete condensation. Figure 2d showed the characteristic Pd 3d spectrum of $\text{PQDs-g-C}_3\text{N}_4$. The binding energies at 340.7 and 335.1 eV could be attributed to Pd 3d_{3/2} and 3d_{5/2}, respectively, which correspond to the Pd⁰. These results confirmed the presence of Pd loads on $g\text{-C}_3\text{N}_4$ surface.

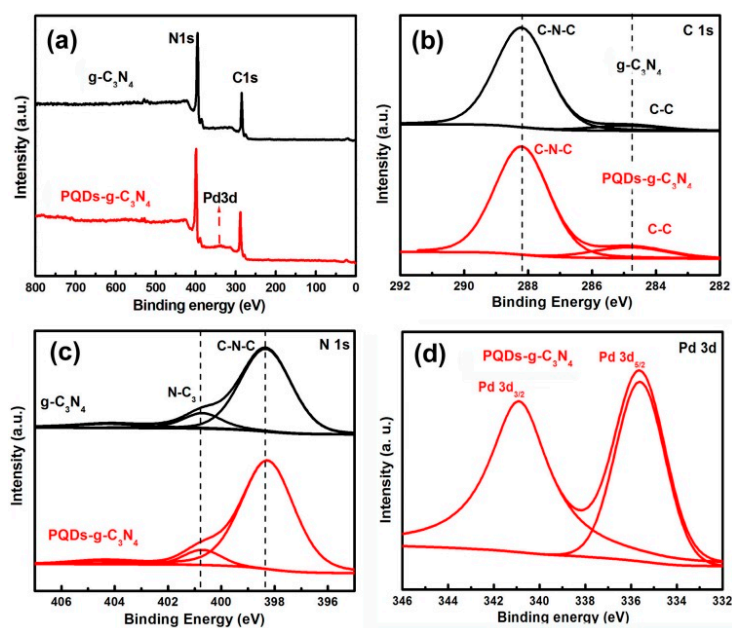


Figure 2. XPS spectra of the results: (a) survey of the sample $g\text{-C}_3\text{N}_4$ and $\text{PQDs-g-C}_3\text{N}_4$; (b) C1s of the sample $g\text{-C}_3\text{N}_4$ and $\text{PQDs-g-C}_3\text{N}_4$; (c) N1s of the sample $g\text{-C}_3\text{N}_4$ and $\text{PQDs-g-C}_3\text{N}_4$; (d) Pd 3d of the sample $g\text{-C}_3\text{N}_4$.

The microstructures of the resulting samples were investigated by TEM. Figure 3 shows the TEM image of $g\text{-C}_3\text{N}_4$ and PQD- $g\text{-C}_3\text{N}_4$. As shown in Figure 3a, the morphology of $g\text{-C}_3\text{N}_4$ was platelet-like. When $g\text{-C}_3\text{N}_4$ was treated in an *in situ* chemical reduction, its morphology was still platelet-like, but with many dark spherical spots on its surface. The dark spherical spots represented Pd-QDs with an average diameter of about 4.5 nm. Figure 3c shows the HRTEM image of PQD- $g\text{-C}_3\text{N}_4$. The lattice spacing of Pd nanoparticles was estimated at 0.228 nm, which corresponds to the (111) plane of Pd.

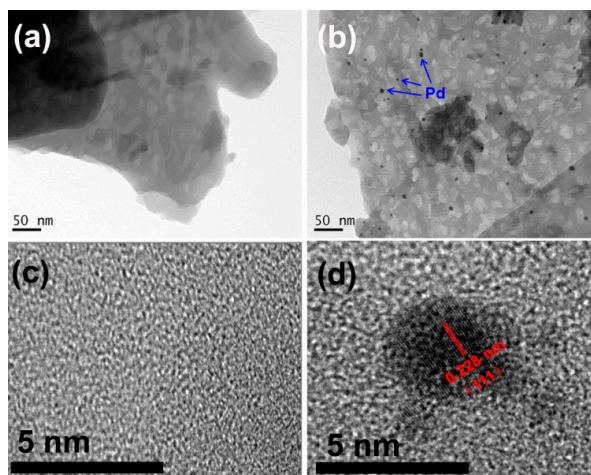


Figure 3. (a) TEM images of $g\text{-C}_3\text{N}_4$ and (b) PQDs- $g\text{-C}_3\text{N}_4$ (Inset: the blue arrows represent Pd QDs) samples; (c) HRTEM images of $g\text{-C}_3\text{N}_4$ and (d) PQDs- $g\text{-C}_3\text{N}_4$ (Inset: the red lines represent the lattice fringes of Pd QDs with d spacing of ca. 0.228 nm) samples.

3.2. Photocatalytic Activities

The photocatalytic activities of the as-prepared $g\text{-C}_3\text{N}_4$ and PQD- $g\text{-C}_3\text{N}_4$ samples were tested in the photocatalytic oxidation of NO under visible light irradiation ($\lambda > 420$ nm). Figure 4 shows the photocatalytic activities of different photocatalysts and NO self-removal in the absence of any photocatalyst. The removal of NO was negligible under visible light irradiation ($\lambda > 420$ nm) without photocatalyst for 40 min, which indicates NO stabilization under visible light irradiation. However, in the presence of the $g\text{-C}_3\text{N}_4$, 34% oxidation efficiency of NO was observed after irradiation for 40 min. Interestingly, the introduction of PQDs remarkably enhanced the removal efficiency of NO, as PQDs- $g\text{-C}_3\text{N}_4$ could remove 72% of NO within 40 min. Obviously, PQD modification could significantly improve the photocatalytic activity of $g\text{-C}_3\text{N}_4$.

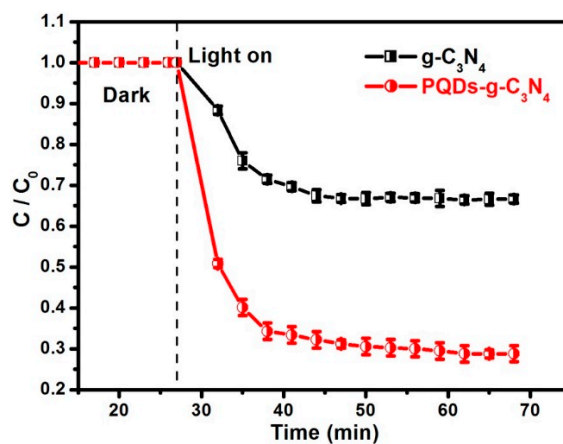


Figure 4. The photooxidation of NO over the samples $g\text{-C}_3\text{N}_4$ and PQDs- $g\text{-C}_3\text{N}_4$ under visible light irradiation ($\lambda > 420$ nm).

3.3. Mechanism of Activity Enhancement

As the photocatalytic activity is often related to the specific surface area, nitrogen sorption was used to measure the surface areas of the resulting samples. However, the measurement results showed that the surface areas of $g\text{-C}_3\text{N}_4$ and PQD- $g\text{-C}_3\text{N}_4$ were 7.9 and 8.2 m^2/g , respectively (Figure 5). Therefore, the enhanced photocatalytic activity of PQDs- $g\text{-C}_3\text{N}_4$ could not be related to the surface area.

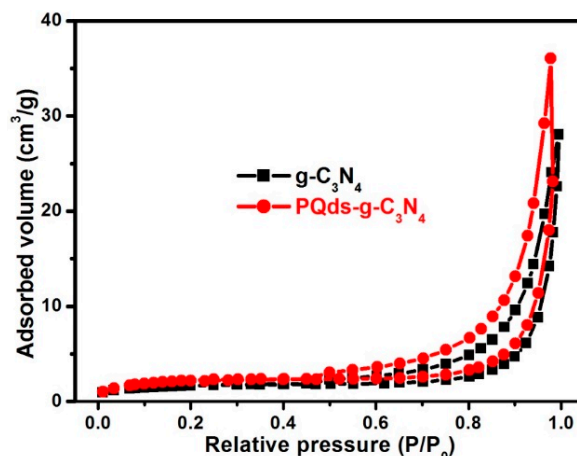


Figure 5. N_2 adsorption-desorption isotherms and Barret–Joyner–Halenda (BJH) pore size distribution plots (inset) of $g\text{-C}_3\text{N}_4$ and PQDs- $g\text{-C}_3\text{N}_4$ samples.

Aside from surface areas, photoabsorption and photoexcitation strongly affect the photocatalytic activity of photocatalysts. We therefore measured UV-VIS absorption spectra of $g\text{-C}_3\text{N}_4$ and PQD- $g\text{-C}_3\text{N}_4$ and found varying absorption edges of the two samples (Figure 6). The intrinsic absorption edge of PQDs- $g\text{-C}_3\text{N}_4$ showed a slight red shift compared to $g\text{-C}_3\text{N}_4$. Meanwhile, the absorption spectra of PQD- $g\text{-C}_3\text{N}_4$ extended to the whole visible light region, even in the infrared region, thereby enhancing light absorbance. This is not surprising, because QD sensitization could increase the light absorption and electronic transmission of photocatalysts. Assuming $g\text{-C}_3\text{N}_4$ is a direct semiconductor, plots of the $(\alpha h\nu)^2$ vs. the energy of absorbed light afford the band gaps of samples, as shown in Figure 6b. The calculated band gaps were approximately 2.75 and 2.62 eV for $g\text{-C}_3\text{N}_4$ and PQDs- $g\text{-C}_3\text{N}_4$, respectively. In such a case, the enhanced light harvesting and narrowed band gap of PQDs- $g\text{-C}_3\text{N}_4$ may result in the formation of more photogenerated electrons.

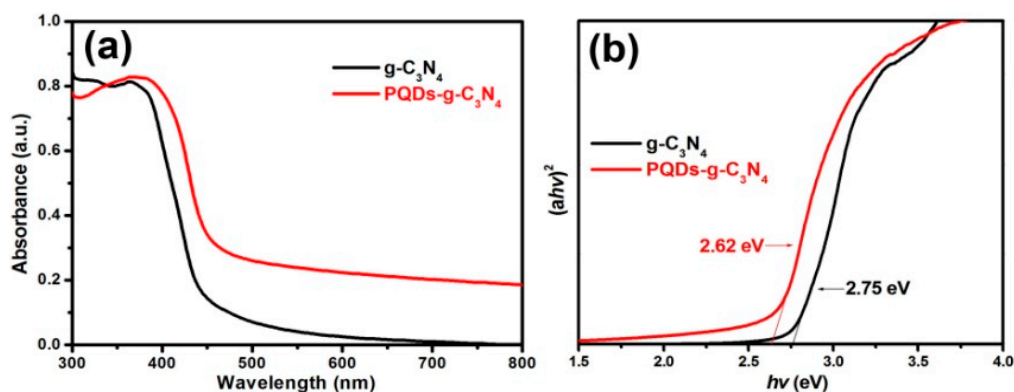


Figure 6. UV-VIS absorption spectra (a) and plots of $(\alpha h\nu)^2$ vs. energy ($h\nu$) (b) of the sample $g\text{-C}_3\text{N}_4$ and PQDs- $g\text{-C}_3\text{N}_4$.

After photoexcitation, the photogenerated electrons may undergo two fates: to migrate to the surface of the photocatalyst for subsequent chemical reactions and to recombine with photogenerated

holes. Photoluminescence (PL) spectra were then used to investigate the recombination and separation of photogenerated electrons and holes in the two samples. Figure 7a displays the PL spectra of $g\text{-C}_3\text{N}_4$ and PQDs- $g\text{-C}_3\text{N}_4$ under the 320-nm excitation. The strong emission peak around 455 nm was derived from the direct electron and hole recombination of the band transition. The weaker PL peak intensity of PQDs- $g\text{-C}_3\text{N}_4$ undoubtedly confirmed that the modification of Pd-QDs could suppress the recombination of photogenerated charge carriers. Generally, photocatalyst with more photogenerated electrons and a lower electron-hole recombination rate would produce a higher photocurrent. Reasonably, the photocurrent that was generated on the PQD- $g\text{-C}_3\text{N}_4$ electrode would be higher than that generated on $g\text{-C}_3\text{N}_4$. This hypothesis could be confirmed by photocurrent measurement (Figure 7b). Therefore, the modification of Pd-QDs would favor the visible light absorption and separation of photogenerated carriers, which would eventually produce more carriers to remove NO.

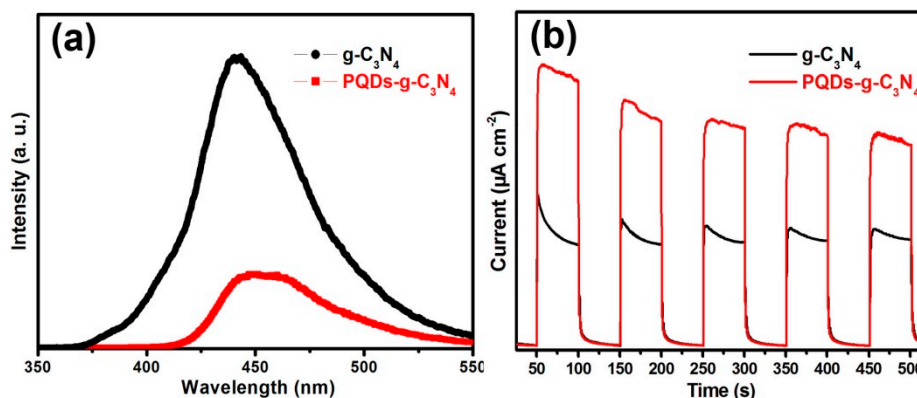
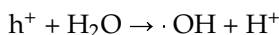
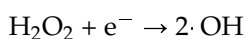
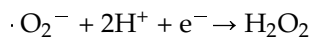
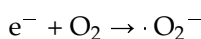


Figure 7. Photoluminescence (PL) spectra of $g\text{-C}_3\text{N}_4$ and PQDs- $g\text{-C}_3\text{N}_4$ (a); current-time curves of $g\text{-C}_3\text{N}_4$ and PQDs- $g\text{-C}_3\text{N}_4$ (b).

3.4. The Mechanism of NO Removal

In general, the photocatalytic removal of NO is attributable to several active species, such as the hydroxyl radicals ($\cdot\text{OH}$), the superoxide ($\cdot\text{O}_2^-$), hydrogen peroxide (H_2O_2) and holes. These active species are formed in the following reactions:



To investigate the possible photocatalytic removal mechanism of NO over $g\text{-C}_3\text{N}_4$ and PQDs- $g\text{-C}_3\text{N}_4$, several experiments were performed to explore this mechanism. Potassium iodide (KI) was used to trap photogenerated holes. As shown in Figure 8, the rate of NO removal over $g\text{-C}_3\text{N}_4$ was suppressed completely when KI was added (5.5% removal efficiency of NO). This result suggests that the hole (h^+) was significant in the photocatalytic removal process of NO on the $g\text{-C}_3\text{N}_4$. Aside from the photogenerated holes, O_2 is an important factor in the photocatalytic process, because it can produce the superoxide ($\cdot\text{O}_2^-$), hydrogen peroxide (H_2O_2) and hydroxyl radicals ($\cdot\text{OH}$). To test the role of dissolved O_2 in degradation, high-purity argon was poured into the reaction to ensure that the reaction was operated without O_2 . As shown in Figure 8, the removal rate of NO on both $g\text{-C}_3\text{N}_4$ (4.7% removal efficiency of NO) and PQDs- $g\text{-C}_3\text{N}_4$ (3.3% removal efficiency of NO) was suppressed

completely, which indicates that O_2 is a necessary factor for NO photocatalytic removal. This result also implies that one or more of three active species ($\cdot O_2^-$, H_2O_2 and $\cdot OH$) are the major contributing factors for the pollutant's degradation. To test this hypothesis, scavengers, such as *p*-benzoquinone (PBQ) for $\cdot O_2^-$ and *tert*-butyl alcohol (TBA) for $\cdot OH$, were utilized in the photocatalytic process of the two samples. As shown in Figure 8a,b, the presence of PBQs could completely inhibit the photocatalytic activity of $g-C_3N_4$ (3.2% removal efficiency of NO); however, it had no effect on NO removal on PQDs- $g-C_3N_4$ (69.1% removal efficiency of NO). Interestingly, the presence of TBA did not influence the NO removal rate of $g-C_3N_4$ (35.8% removal efficiency of NO), but could significantly suppress the NO removal on PQDs- $g-C_3N_4$ (4.5% removal efficiency of NO). As a result, h^+ and $\cdot O_2^-$ have major functions in the removal process of NO on $g-C_3N_4$, whereas $\cdot OH$ plays a major role in the NO removal process over PQDs- $g-C_3N_4$.

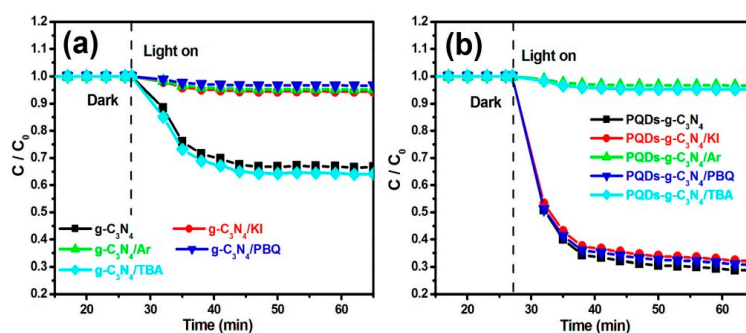


Figure 8. Comparison of NO photoremoval in different photo-catalysis systems under visible light irradiation ($\lambda > 420$ nm): (a) $g-C_3N_4$; (b) PQDs- $g-C_3N_4$. PBQ, *p*-benzoquinone; TBA, *tert*-butyl alcohol.

To find out the reasons for the mechanism change of NO removal induced by the PQDs' modification, we further employed the 5,5-dimethyl-pyrroline *N*-oxide (DMPO) spin-trapping electron spin resonance (ESR) technique to measure the reactive oxygen species, which were generated during photocatalysis. Four characteristic peaks of DMPO- $\cdot O_2^-$ were obviously observed in methanolic suspensions of $g-C_3N_4$ (Figure 9a), which reflects that $\cdot O_2^-$ could be produced via the photocatalysis of $g-C_3N_4$. However, no peaks could be found in the aqueous dispersion of $g-C_3N_4$, which suggests that $\cdot OH^-$ was not generated in the $g-C_3N_4$ system (Figure 9b).

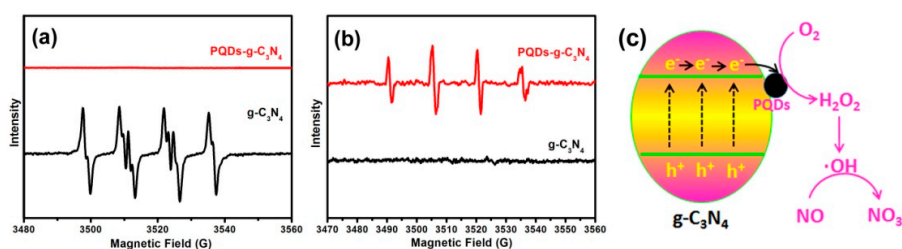


Figure 9. (a) ESR spectra of $g-C_3N_4$ in a methanol aqueous dispersion for DMPO- $\cdot O_2^-$ and in an aqueous dispersion for DMPO- $\cdot OH$; (b) ESR spectra of PQDs- $g-C_3N_4$ in a methanol aqueous dispersion for DMPO- $\cdot O_2^-$ and in an aqueous dispersion for DMPO- $\cdot OH$; (c) $\cdot OH^-$ has major functions in the removal process of NO on PQD- $g-C_3N_4$.

We further measured the DMPO spin-trapping ESR spectra of PQDs- $g-C_3N_4$ in a methanol aqueous dispersion for DMPO- $\cdot O_2^-$ (Figure 9a) and in an aqueous dispersion for DMPO- $\cdot OH$ (Figure 9b). We found that the only $\cdot OH^-$ was generated on PQDs- $g-C_3N_4$. According to previous reports, molecular oxygen can be activated through a single-electron reduction pathway ($e^- \rightarrow \cdot O_2^- \rightarrow H_2O_2 \rightarrow \cdot OH$) or a two-electron reduction pathway ($e^- \rightarrow H_2O_2 \rightarrow \cdot OH$) [31]. Because $\cdot O_2^-$ had not been detected in the PQD- $g-C_3N_4$ system, we therefore believe that PQD modification changed the

molecular oxygen activation pathway from a single-electron reduction to a two-electron reduction. This change was related to the fact that Pd could enhance the oxygen adsorption ability and electron transport performance of PQDs-g-C₃N₄. Therefore, ·O₂[−] has major functions in the removal process of NO on g-C₃N₄, whereas OH[−] has major functions in the removal process of NO on PQD-g-C₃N₄ (Figure 9c).

4. Conclusions

In this study, we developed a practical method to fabricate Pd-QD-modified g-C₃N₄. The modification of Pd-QDs not only favored the visible light absorption of g-C₃N₄, but also improved the separation efficiency of photogenerated carriers and, thus, enhanced the NO photocatalytic oxidation activity. More interestingly, Pd-QD modification changed the NO removal mechanism from the synergistic action of h⁺ and ·O₂[−] to the single action of ·OH. We found that the main reason for the mechanism change was that Pd-QDs modification changed the molecular oxygen activation pathway from single-electron reduction to two-electron reduction. This study could not only develop a novel strategy to modify the Pd-QDs on the surface of photocatalysts, but also shed light on the deep understanding of the relationship between Pd-QD modification and the NO photocatalytic removal activity of semiconductor photocatalysts.

Acknowledgments: This research was financially supported by the research grant of the Early Career Scheme (ECS 809813) from the Research Grant Council, Hong Kong Special Administrative Region (SAR) Government, and Internal Research Grants (R3588) and (R3633) from The Hong Kong Institute of Education.

Author Contributions: Guohui Dong and Wingkei Ho conceived and designed the experiments; Yuhan Li and Liping Yang performed the experiments; Yuhan Li analyzed the data; Guohui Dong and Wingkei Ho contributed reagents/materials/analysis tools; Yuhan Li wrote the paper.

Conflicts of Interest: The authors declare no conflict of interest.

References

1. Fujishima, A.; Honda, K. Electrochemical photolysis of water at a semiconductor electrode. *Nature* **1972**, *238*, 37–38. [[CrossRef](#)] [[PubMed](#)]
2. Hoffmann, M.R.; Martin, S.T.; Choi, W.; Bahnemann, D.W. Environmental applications of semiconductor photocatalysis. *Chem. Rev.* **1995**, *95*, 69–96. [[CrossRef](#)]
3. Carraway, E.R.; Hoffman, A.J.; Hoffmann, M.R. Photocatalytic oxidation of organic acids on quantum-sized semiconductor colloids. *Environ. Sci. Technol.* **1994**, *28*, 786–793. [[CrossRef](#)] [[PubMed](#)]
4. Marta, I.L. Heterogeneous photocatalysis transition metal ions in photocatalytic systems. *Appl. Catal. B* **1999**, *23*, 89–114.
5. Fujishima, A.; Rao, T.N.; Tryk, D.A. Titanium dioxide photocatalysis. *J. Photochem. Photobiol. C* **2000**, *1*, 1–21. [[CrossRef](#)]
6. Yamasita, D.; Takata, T.; Hara, M.; Kondo, J.N.; Domen, K. Recent progress of visible-light-driven heterogeneous photocatalysts for overall water splitting. *Solid State Ion.* **2004**, *172*, 591–595. [[CrossRef](#)]
7. Ettetdgui, J.; Diskin-Posner, Y.; Weiner, L.; Neumann, R. Photoreduction of carbon dioxide to carbon monoxide with hydrogen catalyzed by a Rhenium(I) phenanthroline-polyoxometalate hybrid complex. *J. Am. Chem. Soc.* **2011**, *133*, 188–190. [[CrossRef](#)] [[PubMed](#)]
8. Zhang, L.; Wang, W.; Jiang, D.; Gao, E.; Sun, S. Photoreduction of CO on BiOCl nanoplates with the assistance of photoinduced oxygen vacancies. *Nano Res.* **2015**, *3*, 821–831. [[CrossRef](#)]
9. Kim, Y.I.; Salim, S.; Huq, M.J.; Mallouk, T.E. Visible light photolysis of hydrogen iodide using sensitized layered semiconductor particles. *J. Am. Chem. Soc.* **1991**, *113*, 9561–9563. [[CrossRef](#)]
10. Lee, Y.; Terashima, H.; Shimodaira, Y.; Teramura, K.; Hara, M.; Kobayashi, H.; Domen, K.; Yashima, M. Zinc germanium oxynitride as a photocatalyst for overall water splitting under visible light. *J. Phys. Chem. C* **2007**, *111*, 1042–1048. [[CrossRef](#)]
11. Maeda, K.; Takata, T.; Hara, M.; Saito, N.; Inoue, Y.; Kobayashi, H.; Domen, K. GaN:ZnO solid solution as a photocatalyst for visible-light-driven overall water splitting. *J. Am. Chem. Soc.* **2005**, *127*, 8286–8287. [[CrossRef](#)] [[PubMed](#)]

12. Hitoki, G.; Takata, T.; Kondo, J.N.; Hara, M.; Kobayashi, H.; Domen, K. An oxynitride, TaON, as an efficient water oxidation photocatalyst under visible light irradiation ($\lambda < 500$ nm). *Chem. Commun.* **2002**, *16*, 1698–1699.
13. Wang, X.W.; Maeda, K.; Thomas, A.; Takanabe, K.; Xin, G.; Carlsson, J.M.; Domen, K.; Antonietti, M. A metal-free polymeric photocatalyst for hydrogen production from water under visible light. *Nat. Mater.* **2009**, *8*, 76–80. [[CrossRef](#)] [[PubMed](#)]
14. Chen, X.F.; Zhang, J.S.; Fu, X.Z.; Antonietti, M.; Wang, X.C. Fe-g-C₃N₄-Catalyzed oxidation of benzene to phenol using hydrogen peroxide and visible light. *J. Phys. Chem. A* **2009**, *131*, 11658–11659. [[CrossRef](#)] [[PubMed](#)]
15. Ding, Z.X.; Chen, X.F.; Antonietti, M.; Wang, X.C. Synthesis of transition metal-modified carbon nitride polymers for selective hydrocarbon oxidation. *ChemSusChem* **2010**, *4*, 274–281. [[CrossRef](#)] [[PubMed](#)]
16. Yan, S.C.; Li, Z.S.; Zou, Z.G. Photodegradation of rhodamine b and methyl orange over boron-doped g-C₃N₄ under visible light irradiation. *Langmuir* **2010**, *26*, 3894–3910. [[CrossRef](#)] [[PubMed](#)]
17. Dong, G.H.; Ai, Z.H.; Zhang, L.Z. Efficient anoxic pollutant removal with oxygen functionalized graphitic carbon nitride under visible light. *RSC Adv.* **2014**, *4*, 5553–5560. [[CrossRef](#)]
18. Dong, G.H.; Ho, W.K.; Li, Y.H.; Zhang, L.Z. Facile synthesis of porous graphene-like carbon nitride (C₆N₉H₃) with excellent photocatalytic activity for NO removal. *Appl. Catal. B Environ.* **2015**, *174*, 477–485. [[CrossRef](#)]
19. Liu, G.; Niu, P.; Sun, C. Unique electronic structure induced high photoreactivity of sulfur-doped graphitic C₃N₄. *J. Am. Chem. Soc.* **2010**, *132*, 11642–11648. [[CrossRef](#)] [[PubMed](#)]
20. Dong, G.H.; Zhang, L.Z. Synthesis and enhanced Cr(VI) photoreduction property of formate anion containing graphitic carbon nitride. *J. Phys. Chem. C* **2013**, *117*, 4062–4068. [[CrossRef](#)]
21. Liu, J.; Liu, Y.; Liu, N.; Kang, Z. Metal-free efficient photocatalyst for stable visible water splitting via a two-electron pathway. *Science* **2015**, *347*, 970–974. [[CrossRef](#)] [[PubMed](#)]
22. Lin, Z.; Xue, W.; Chen, H.; Lin, J.M. Peroxynitrous-acid-induced chemiluminescence of fluorescent carbon dots for nitrite sensing. *Anal. Chem.* **2011**, *83*, 8245–8251. [[CrossRef](#)] [[PubMed](#)]
23. Di, J.; Xia, J.; Ji, M.; Li, H.; Hui, X.; Chen, R. The synergistic role of carbon quantum dots for the improved photocatalytic performances of Bi₂MoO₆. *Nanoscale* **2015**, *7*, 11433–11443. [[CrossRef](#)] [[PubMed](#)]
24. Li, G.S.; Zhang, D.Q.; Yu, J.C. A new visible-light photocatalyst: CdS quantum dots embedded mesoporous TiO₂. *Environ. Sci. Technol.* **2009**, *43*, 7079–7085. [[CrossRef](#)] [[PubMed](#)]
25. Leutwyler, W.K.; Bürgi, S.L.; Burgli, H. Semiconductor clusters, nanocrystals, and quantum dots. *Science* **1996**, *271*, 933–937.
26. Shen, J.; Zhu, Y.; Yang, X.; Li, C. Graphene quantum dots: emergent nanolights for bioimaging, sensors, catalysis and photovoltaic devices. *Chem. Commun.* **2012**, *48*, 3686–3699. [[CrossRef](#)] [[PubMed](#)]
27. Liu, Q.; Zhang, J. Graphene supported Co-g-C₃N₄ as a novel metal-macrocylic electrocatalyst for the oxygen reduction reaction in fuel cells. *Langmuir* **2013**, *29*, 3821–3828. [[CrossRef](#)] [[PubMed](#)]
28. Samanta, S.; Martha, S.; Parida, K. Facile synthesis of Au/g-C₃N₄ nanocomposites: an inorganic/organic hybrid plasmonic photocatalyst with enhanced hydrogen gas evolution under visible-light irradiation. *ChemCatChem* **2014**, *6*, 1453–1462. [[CrossRef](#)]
29. Shalom, M.; Guttentag, M.; Fettkenhauer, C.; Inal, S.; Neher, D.; Llobet, A.; Antonietti, M. *In situ* formation of heterojunctions in modified graphitic carbon nitride: Synthesis and noble metal free photocatalysis. *Chem. Mater.* **2014**, *26*, 5812–5818. [[CrossRef](#)]
30. Dong, G.H.; Zhang, L.Z. Porous structure dependent photoreactivity of graphitic carbon nitride under visible light. *J. Mater. Chem.* **2012**, *22*, 1160–1166. [[CrossRef](#)]
31. Dong, G.H.; Ai, Z.H.; Zhang, L.Z. Total aerobic destruction of azo contaminants with nanoscale zero-valent copper at neutral pH: Promotion effect of in-situ generated carbon center radicals. *Water Res.* **2014**, *66*, 22–30. [[CrossRef](#)] [[PubMed](#)]

Sample Availability: Samples are available from the authors.



© 2015 by the authors; licensee MDPI, Basel, Switzerland. This article is an open access article distributed under the terms and conditions of the Creative Commons by Attribution (CC-BY) license (<http://creativecommons.org/licenses/by/4.0/>).